Hindawi Publishing Corporation
Advances in Meteorology
Volume 2016, Article ID 5375918, 13 pages
http://dx.doi.org/10.1155/2016/5375918

Research Article

Statistical Analysis of Relationship between Daytime Lidar-Derived Planetary Boundary Layer Height and Relevant Atmospheric Variables in the Semiarid Region in Northwest China

Ruijun Dang,[1] Hong Li,[1] Zhiguo Liu,[2] and Yi Yang[1]

[1]*Key Laboratory of Arid Climatic Changing and Reducing Disaster of Gansu Province, College of Atmospheric Sciences, Lanzhou University, Lanzhou, Gansu 730000, China*
[2]*The Central Meteorological Observatory of Lanzhou, Lanzhou 730020, China*

Correspondence should be addressed to Yi Yang; yangyi@lzu.edu.cn

Received 9 November 2015; Revised 19 January 2016; Accepted 18 April 2016

Academic Editor: Jose D. Fuentes

Accurate identification of key parameters for data assimilation is important in simulating the planetary boundary layer height (PBLH) and structure evolution in numerical weather prediction models. In this study, surface observational data and lidar-derived PBLH on 42 cloudless days from June 2007 to May 2008 are used to quantify the statistical relationships between surface parameters and the PBLH at a semiarid climate observational site in Northwest China. The results indicate that surface upward long wave radiation, surface temperature, and surface sensible heat fluxes show strong correlations with the PBLH with correlation coefficients at a range of 0.63–0.72. But these parameters show varying correlation response time to the different stages of PBL development. Furthermore, the air temperature shows the highest correlation with the PBLH near the surface and the correlation decreases with increasing height.

1. Introduction

The atmospheric boundary layer, also known as the planetary boundary layer (PBL), is the turbulent layer near the Earth's surface. It is directly affected by the underlying surface conditions and intimately associated with human activities [1]. The transfers of momentum, heat, and moisture between the surface and atmosphere are mainly based on turbulence. As the atmosphere is always in turbulent status in the layer, the PBL is crucial to surface-atmosphere exchanges of substances and energy. PBLH is of major relevance in boundary layer research as a key parameter characterizing the structure of the boundary layer [2, 3]. Observations of the PBLH are significant for theory and applications. Because it is closely related to turbulence, the PBLH is not observed by standard measurements. It is currently determined mainly from indirect measurements. For a convective boundary layer at noon, the PBLH is more or less identical with the mixed layer height. Due to the vertical turbulent mixing, wind velocity and potential temperature are well mixed within the layer. In most cases, wind and potential temperature are usually constants in the mixed layer. However, at the top of mixed layer, there is a sharp increase in wind speed and potential temperature caused by the abrupt decrease in turbulence intensity [4]. Therefore, the characteristics of wind speed and potential temperature can be used to calculate the PBLH when atmosphere is neutral or unstable. In addition, the PBL is moist relative to the upper free atmosphere, and a strong gradient in relative humidity exists at the top of PBL, which can also be utilized to determine the daytime PBLH [5]. At night when atmosphere is in a stable condition, inversion lid always exists at the top of boundary layer, and the nocturnal PBLH is usually represented by the thickness of surface temperature inversion layer. Above all, the PBLH can be determined from different instruments-derived profiles of thermodynamic variables like temperature, humidity, and

horizontal wind speed. The difficulty in directly observing the thermodynamic structures of the atmosphere makes ground-based remote sensing technique an attractive choice. For instance, lidar provides vertical profiles of backscatter from aerosol particles with high temporal and spatial resolutions in the atmosphere. The aerosol concentration within the PBL is much higher than that in the free atmosphere. Therefore, a significant difference in aerosol concentration exists between the top of the PBL and the free atmosphere, which is reflected as a sudden attenuation of the lidar echo signals. On the basis of this characteristic of aerosols in the PBL, aerosol particles can be used as tracers to determine the PBLH. However, in the presence of optically thick clouds, the resulting PBLH using lidar data is unrealistic because of the high signal gradient generated by the clouds [6, 7]. Therefore, lidar data in clear sky conditions are chosen to calculate PBLH in this paper.

As the backscatter signal generally decreases most rapidly at the top of the boundary layer, the gradient of the aerosol concentration obtained from the lidar data can be utilized to retrieve PBLH. Many methods have been used to calculate the PBLH from lidar backscatter, including the gradient method [8, 9], the wavelet transform method [10–12], the standard deviation method [13], and the curve fitting method [14, 15]. Each method has its advantages and limitations. The gradient method is simple and easy to use; however, it is sensitive to local minima in the profile either atmosphere or noise induced nearly always occurring in a turbulent PBL [16]. The standard deviation method is not suitable for the situation of weak inversion layer [17]. Although the curve fitting method is relatively computationally expensive, it is barely affected by the local structure of the signal and generally generates the stable PBLH [14]. Therefore, the curve fitting method is used to retrieve daytime PBLH in the paper.

The atmospheric boundary layer is largely governed by land surface processes, including the absorption of solar radiation by the land surface, transmission of heat energy between the atmosphere and soil, and mechanical processes. The surface temperature is an important external forcing factor to the thermal convection. The variation in surface temperature reflects the heating result of net radiation on the surface [18]. For net radiation, the contribution of the long and short wave components varies with atmospheric conditions. On sunny days, the upward long wave contributes most to the net radiation, and the contribution of upward short wave is minimum [19]. Besides, the development and maintenance of the thermal boundary layer mainly rely on the heat transmission through the sensible heat flux [20]. Therefore, the radiation variables, surface temperature, and sensible heat flux make major contributions to the formation and development of the PBL [21–24]. The assimilation of PBLH may be implemented by updating the first guess field of a numerical model with these variables.

For PBLH assimilation in the numerical model with Ensemble Kalman Filter (EnKF), it needs to confirm which variables are well correlated with PBLH. In addition, the influence radius for spatial and temporal domain should also be set. So the purpose of this study is to determine the statistical correlations between PBLH and conventional atmospheric variables, as well as influence radius of variables using the routine observations at the Semi-Arid Climate and Environment Observatory of Lanzhou University (SACOL) and to provide basis and support for PBLH assimilation. Due to the limitation of a single observational point, the radius of influence in horizontal direction cannot be found out. In the vertical direction, the vertical air temperature profiles are provided by a Radiometrics Profiling Radiometer (TP/WVP-3000). The observations of variables and PBLH in the following hours are used to analyze the temporal influence radius.

In this study, 42 cloudless sunny days (nonprecipitation, being without thunderstorm, no cloud or total-cloud covers less than 20 percent all day, and being with a clear structure of backscatter signals of lidar) are selected from June 2007 to May 2008, and the PBLH is calculated by retrieving lidar data using the curve fitting method over the Lanzhou suburb in the Yuzhong area at SACOL. The correlations between related variables and PBLH as well as lagged correlations between them are calculated to determine the major variables which affect the formation and development of boundary layer. The correlation coefficients between PBLH and air temperature at different heights are also calculated. Finally, through temporal variations of PBLH and atmospheric variables on the four typical examples 15 July 2007, 20 November 2007, 5 January 2008, and 9 April 2008, the lagged correlations between different variables and PBLH and the physical mechanisms behind the statistical correlations are specifically discussed.

2. Data and Methods

The PBLH and statistical correlations in this paper are calculated with data collected at SACOL (35.57°N, 104.08°E; 1965.8 m above sea level), which is the suburb of Lanzhou on the southern bank of the Yellow River, a typical semiarid region. The instruments include air temperature and relative humidity sensors (HMP45C-L, Vaisala), a Precision Infrared Thermocouple Sensor (IRTS-P, Apogee), upward and downward pyranometers (CM21, Kipp & Zonen), upward and downward pyrgeometers (CG4, Kipp & Zonen), an atmospheric pressure sensor (RPT410F-3143, Druck), a Radiometrics Profiling Radiometer (TP/WVP-3000, Radiometrics), and a Micro-Pulse Lidar System (MPL-4, Sigma Space). The vertical resolutions of temperature profiles measured by the radiometer for the layers 1 km below and above are 100 m and 250 m, respectively. MPL-4 has one measurement channel at 527 nm, which records backscatter signals up to a height of 20+ km with a vertical resolution of 75 m. All the conventional atmospheric observations are subjected to basic quality control (QC). Only observations with a relatively high accuracy are selected. The SACOL MPL-4 is part of the MPLNET (Micro-Pulse Lidar Network) [25], and the observation follows the relevant uniform rules. Meanwhile, a series of corrections such as background correction, overlap correction, and range correction have been done for lidar data [26].

The curve fitting method first proposed by Steyn et al. [14] is used to retrieve PBLH from the lidar data. The technique uses the gradient of the lidar backscatter signal and fits an idealized backscatter profile $B(z)$ to the observed backscatter profile $b(z)$ by minimizing the measure of agreement between

the two profiles. The form of the idealized backscatter profile $B(z)$ is

$$B(z) = \frac{(B_m + B_u)}{2} - \frac{(B_m - B_u)}{2} \operatorname{erf}\left(\frac{z - Z_m}{S}\right), \quad (1)$$

where the error function (erf) is defined as

$$\operatorname{erf}(a) = \frac{2}{\sqrt{\pi}} \int_0^a \exp\left(-z^2\right) dz, \quad (2)$$

where B_m and B_u are the mean backscatters in the mixed layer and in air immediately above the mixed layer, respectively; Z_m is the depth of the mixed layer; S is related to the thickness of the entrainment layer. The four parameters are determined by minimizing the root-mean-square deviation between $B(z)$ and $b(z)$. When the root-mean-square deviation gets the minimum, Z_m represents the PBLH.

3. Statistical Correlations between PBLH and Variables

3.1. Statistical Correlations between Averages. The dates chosen for PBLH retrieval and correlation analysis are listed in Table 1. On these 42 cloudless sunny days, conventional observations are complete. The structure of the lidar backscatter signals is also very clear. To ensure representativeness, the selected days are from all four seasons. Because some data are unavailable for 8–30 September 2007, the cases in autumn are relatively less. But the representativeness of the statistical correlations is not affected.

Table 2 lists the Pearson correlation coefficients of the averages of different variables and PBLH during 10:00 and 18:00 BJT (Beijing time). It shows strong correlations between individual thermal variables (e.g., surface air temperature, surface temperature, sensible heat flux, and upward and downward long wave and short wave radiation) and PBLH, with correlation coefficients all around 0.6 (significant at the 0.01 level). Surface relative humidity and atmospheric pressure are negatively correlated with PBLH, but their relevance is relatively low, and the Pearson correlation coefficients are −0.34 and −0.25, respectively. The weakest correlation is between averages of net radiation and PBLH. Figure 1 shows the distribution of averages of variables and PBLH. It can be seen that the daily average of net radiation changes very little, while the PBLH shows a clear change (see Figure 1(b)). The overall trends of atmospheric pressure and surface relative humidity are opposite to that of PBLH although they change in tandem with PBLH sometimes (see Figure 1(c)). Apart from these three variables, Figure 1 shows that the overall trends of other variables are fairly consistent with the trend of PBLH.

3.2. Statistical Correlations between Time Series. In general, the atmospheric boundary layer appears as a convective layer in daytime and a stable boundary layer at night. Ding [27] discussed that the boundary layer with a thick mixed layer is relatively stable before sunrise in Northwest China. After 08:00 BJT, the nighttime stable boundary layer is broken, and the mixed layer starts to deepen. Around 10:00 BJT, because of the thermally driven vertical mixing, the residual layer starts to disappear and the mixed layer begins to develop rapidly. At noon, the convective boundary layer is established. Zhao et al. [28] estimated the PBLH in summer over the SACOL using lidar measurements and a numerical model and showed that the deepest boundary layer over SACOL occurred at around 17:00 BJT and could last until 18:00 BJT. Therefore, the PBLH during 10:00–18:00 BJT and atmospheric variables during 06:00–14:00, 07:00–15:00, 08:00–16:00, 09:00–17:00, and 10:00–18:00 BJT are selected as time series to analyze the lagged statistical correlations between variables and daytime PBLH as the PBLH often lags behind these variables.

Statistical correlations between different atmospheric variables and PBLH with a lag of 1, 2, 3, and 4 hours are listed in Table 3. There are significant correlations between thermal variables (except net radiation) and PBLH with Pearson correlation coefficients all above 0.6 (significant at the 0.01 level), which are highly consistent with the results shown in

Table 1: The days selected for retrieving PBLH and for correlation analysis between PBLH and atmospheric variables from June 2007 to May 2008.

June	July	Aug	Nov	Dec	Jan	Feb	Mar	Apr	May
1	15	14	20	19	5	20	1	2	4
9	16	16	22	20	9	21	3	4	5
	22	19	28	22	15		13	6	11
		31	30				25	9	14
							26	17	26
								24	28
								25	31
								27	
								28	

Table 2: Statistical correlations between the averages of atmospheric variables and boundary layer height during 10:00 and 18:00 BJT (T_0: surface air temperature; T_s: surface temperature; H: sensible heat flux; RH: surface relative humidity; P: atmospheric pressure; R_{lu}, R_{su}, R_{ld}, and R_{sd}: upward long wave and short wave radiation and downward long wave and short wave radiation, resp.; R_n: net radiation; r: Pearson correlation coefficient).

Variables	r
T_0	0.71^{**}
T_s	0.71^{**}
H	0.63^{**}
RH	-0.34^{*}
P	−0.25
R_{lu}	0.75^{**}
R_{ld}	0.55^{**}
R_{sd}	0.76^{**}
R_{su}	0.60^{**}
R_n	−0.04

*Significant correlation at the 0.05 significance level.
**Significant correlation at the 0.01 significance level.

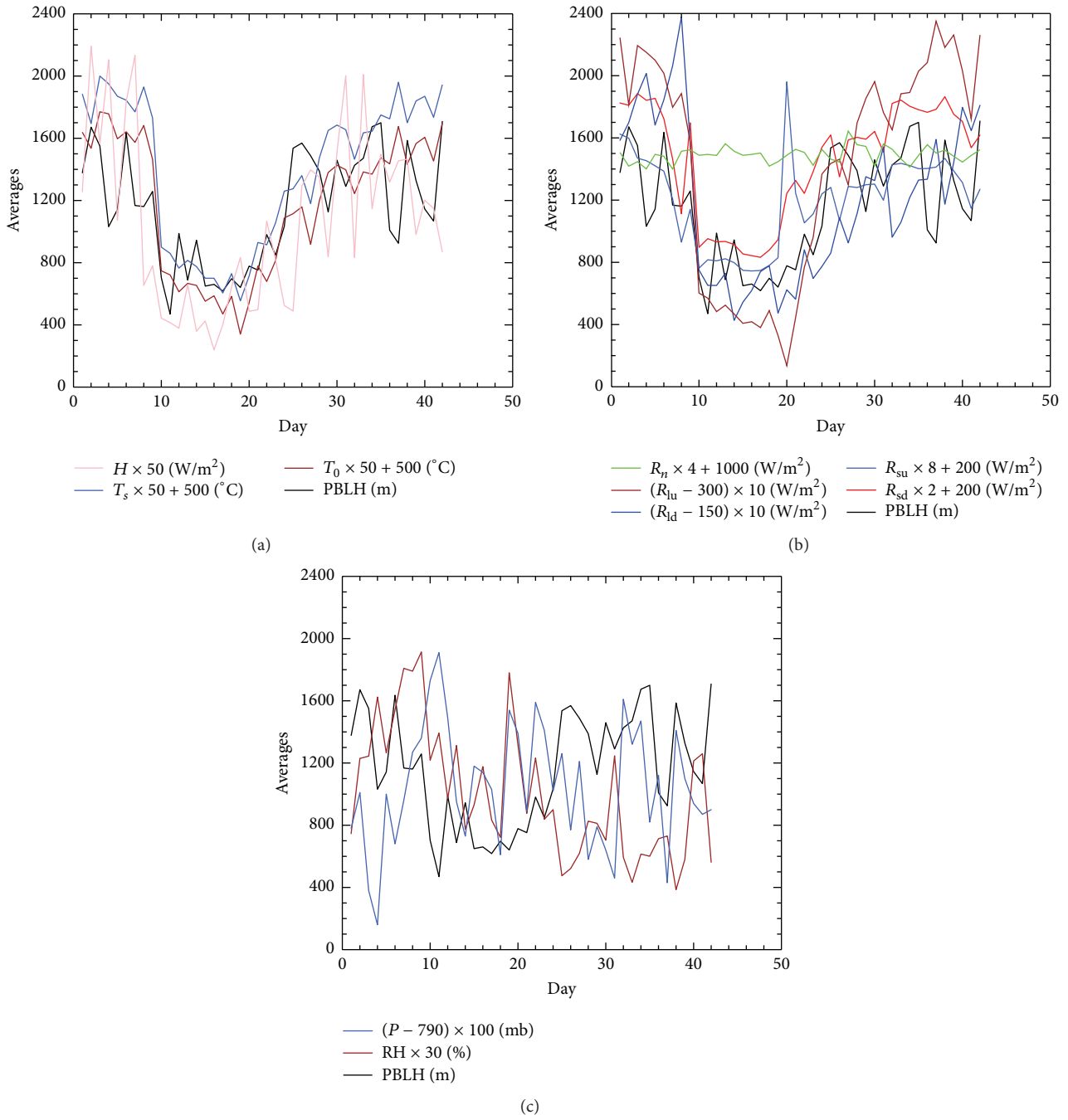

FIGURE 1: Distribution of daily averages of atmospheric variables and boundary layer height for 42 selected days (see Table 2 for abbreviations).

Table 2. It is also clear that stronger significant correlations exist between variables and the PBLH 2-3 hours later. The Pearson correlation coefficients between surface temperature, surface air temperature, and PBLH 2 hours later are 0.70 and 0.68, respectively. Upward long wave radiation, upward short wave radiation, and downward short wave radiation are more highly correlated with PBLH 3 hours later. The correlation coefficients are 0.72, 0.69, and 0.61, respectively. Downward long wave radiation is different from the others. It is more highly correlated with PBLH at the same time. Besides, with the correlation coefficient of 0.63, sensible heat flux highly correlates with PBLH at the same time or about 1 hour later. Among radiation variables, net radiation correlates worst with PBLH. However, the PBLH that lags 3 hours still correlates with net radiation significantly with the correlation coefficient of 0.45. PBLH is negatively correlated with both atmospheric pressure and surface relative humidity, although the correlations are not as significant as those with above thermal variables. For the lagging effect, the PBLH changes about 2 hours after a change in relative humidity.

Table 3: Statistical correlations between different atmospheric variables and PBLH with a delay of 1–4 hours (T_0: surface air temperature; T_s: surface temperature; H: sensible heat flux; RH: surface relative humidity; P: atmospheric pressure; R_{lu}, R_{su}, R_{ld}, and R_{sd}: upward long wave and short wave radiation and downward long wave and short wave radiation, respectively; R_n: net radiation; r: Pearson correlation coefficient).

Variables	At the same time	PBLH 1 h later	PBLH 2 h later	PBLH 3 h later	PBLH 4 h later
	r	r	r	r	r
T_0	0.65**	0.67**	0.68**	0.68**	0.67**
T_s	0.68**	0.70**	0.70**	0.70**	0.68**
H	0.63**	0.63**	0.61**	0.57**	0.52**
RH	−0.41**	−0.43**	−0.43**	−0.41**	−0.37**
P	−0.31**	−0.29**	−0.25**	−0.20**	−0.16**
R_{lu}	0.57**	0.67**	0.72**	0.72**	0.71**
R_{ld}	0.51**	0.51**	0.50**	0.48**	0.46**
R_{sd}	0.29**	0.54**	0.68**	0.69**	0.66**
R_{su}	0.17**	0.41**	0.57**	0.61**	0.60**
R_n	−0.15**	0.18**	0.40**	0.45**	0.43**

** Significant correlation at the 0.01 significance level.

To identify any relation and influence radius in the vertical direction, Table 4 shows the statistical correlations between PBLH and air temperature at different heights for different times. At 10:00 BJT, only air temperature below 1000 m is correlated with PBLH, but after 12:00 BJT, air temperature within 5000 m is significantly correlated with PBLH. In addition, the highest correlation between PBLH and air temperature below (above) 1000 m occurs at 12:00 (14:00) BJT, and the Pearson correlation coefficient is 0.75 (0.64). Thermal forcing is the driving factor for the development of daytime mixed layer (10:00–18:00 BJT). However, only small amount of solar radiation is absorbed by air in the boundary layer; most (about 90%) is delivered to the surface. In turn it forces development of PBL through turbulent transport. In the vertical direction, the forcing effect of surface decreases with height, and temporal variation in air temperature at higher altitude is less significant [1]. So the Pearson correlation coefficient between air temperature and PBLH is highest at the surface and decreases with height for all times. Also, the air temperature correlates with PBL most significantly at noon when thermal turbulent transport is strongest. Additionally, for the whole troposphere, the ground surface is the main heat source, so the air temperature in the free atmosphere also changes with the surface condition. Therefore, at 14:00 BJT, there is still a relatively higher correlation between PBLH and air temperature at 5 km.

4. Cases Analysis

To verify the statistical lagged correlations between variables and PBL and discuss the physical mechanisms behind these statistical results, the four cloudless sunny days 09 April 2008, 15 July 2007, 20 November 2007, and 5 January 2008 are selected as typical spring, summer, fall, and winter examples for analysis.

4.1. Synoptic Condition. Besides surface processes, synoptic condition is also an important factor contributing to the overall height of boundary layer. The surface pressures at 14:00 BJT of four cases are shown in Figure 2. And Figure 3 shows the time-altitude cross section of the backscatter intensity, and the red line represents the retrieved PBLH with the curve fitting method. From Figures 2(a) and 2(b), Yuzhong region is controlled by weak low-surface pressure at 14:00 BJT on 9 April 2008 and 15 July 2007. The synoptic condition is good for PBL development. According to Figures 3(a) and 3(b), the highest PBLH are 1850 m and 2150 m on the two cloudless sunny days, which are relatively higher than on other two cases. From Figures 2(c) and 2(d), it can be seen that the area is controlled by the edge of high-pressure system at 14:00 BJT on 20 November 2007 and 5 January 2008, which indicates an aloft airflow convergence and a surface divergence. In these cases, the PBL developments are subsided and restricted; the highest PBLH are 1100 m and 860 m, respectively (see Figures 3(c) and 3(d)). Meanwhile, Figure 3 also shows the times when PBLH get the maximum. The times of the peak values are 17:30, 15:30, 17:00, and 17:00 BJT, respectively. It is not difficult to understand that the difference on temporal variation in PBLH in different cases is closely related to the difference on the land surface processes and the variation in atmospheric variables. In addition, the difference between the heights at which the signals reduce fastest and the retrieved PBLH (red lines) is small (Figure 3), and the corresponding times are also fairly consistent, which support the reason of choosing the curve fitting method for retrieving PBLH on sunny days. Before 10:00 BJT on 9 April 2008 and 15 July 2007 (Figures 3(a) and 3(b)), the retrieved boundary layer heights are relatively higher, which may be caused by cloud or the limitation of the method.

4.2. Temporal Variation Analysis. The temporal variations in radiation variables are plotted in Figure 4. The downward short wave radiation is the part of solar radiation that reaches the surface after being attenuated by atmosphere. Then some is absorbed by the surface and the rest is reflected back into the atmosphere, which is upward short wave radiation. Therefore, to all cases, the upward short wave radiation always accompanies the downward component and has a smaller

Table 4: Statistical correlations between PBLH and air temperature at different heights and at different times (r: Pearson correlation coefficient).

Height	10:00	12:00	14:00	16:00	18:00
(m)	r	r	r	r	r
0	0.57**	0.75**	0.66**	0.64**	0.63**
100	0.55**	0.74**	0.66**	0.64**	0.62**
200	0.53**	0.73**	0.65**	0.63**	0.61**
300	0.52**	0.72**	0.65**	0.62**	0.60**
400	0.48**	0.71**	0.65**	0.61**	0.59**
500	0.45**	0.70**	0.65**	0.60**	0.58**
600	0.41**	0.68**	0.64**	0.59**	0.57**
700	0.39*	0.67**	0.64**	0.57**	0.56**
800	0.36*	0.65**	0.64**	0.56**	0.55**
900	0.34*	0.64**	0.64**	0.55**	0.54**
1000	0.32*	0.63**	0.64**	0.54**	0.53**
1250	0.28	0.59**	0.63**	0.50**	0.50**
1500	0.25	0.58**	0.63**	0.48**	0.48**
1750	0.26	0.57**	0.63**	0.48**	0.48**
2000	0.26	0.57**	0.63**	0.47**	0.47**
2250	0.25	0.56**	0.62**	0.46**	0.46**
2500	0.26	0.56**	0.62**	0.46**	0.46**
2750	0.25	0.55**	0.62**	0.45**	0.45**
3000	0.26	0.55**	0.62**	0.45**	0.45**
3250	0.25	0.54**	0.61**	0.43**	0.43**
3500	0.25	0.54**	0.61**	0.43**	0.43**
3750	0.24	0.53**	0.60**	0.42**	0.42**
4000	0.25	0.53**	0.60**	0.42**	0.42**
4250	0.25	0.53**	0.60**	0.42**	0.42**
4500	0.25	0.53**	0.60**	0.41**	0.41**
4750	0.25	0.53**	0.60**	0.41**	0.41**
5000	0.25	0.53**	0.59**	0.41**	0.41**

*Significant correlation at the 0.05 significance level.
**Significant correlation at the 0.01 significance level.

value than the latter one. From Figure 4, it is obvious that in the first two cases short wave radiations have higher values than on 20 November 2007 and 5 January 2008, which is caused by the seasonal variation of solar altitude angles (atmospheric transparency is not considered in cloudless sunny days). Except the synoptic condition, as the ultimate source of energy, short wave radiation contributes to the difference on overall PBLH to a certain extent. In addition, for temporal variation, the downward and upward short wave radiations reach their maximum values between 12:30 and 13:30 and then decrease rapidly. The lag time of PBLH is less than 3 hours on 15 July 2007 and more than 3 hours for the other three cases. Obviously, for different cases, although the temporal variations in short wave radiation are similar, significant differences exit at the development and lag time of PBLH. The differences may be caused by differences on land process in different seasons.

The upward long wave radiation mainly depends on surface temperature. After the arrival of solar radiation, the surface is heated and surface temperature increases gradually until it gets the maximum. Therefore, the time that the upward long wave radiation gets the peak value is a little later than that of the short wave radiation. In the case of 15 July 2007, the value of the upward long wave radiation is biggest, and in the case of 5 January 2008 it is smallest. In the other two cases, the values are in between. The peak values of the upward long wave radiation occur between 13:30 and 14:30, indicating that the lag times of PBLH are 3.5, 1.5, 3.5, and 2.5 hours, respectively. The temporal variation in downward long wave radiation is different from other radiation components. To all cases, the variable increases until about 18:00 or begins to decrease after 17:00. Besides, the temporal variation range of downward long wave radiation is also smaller than others. The atmosphere absorbs both short wave and long wave radiation, but only 15%–25% of the short wave radiation is absorbed, and the atmosphere mainly absorbs long wave radiation. After greenhouse gases such as water vapor and carbon dioxide in atmosphere absorb the long wave radiation, the atmosphere is exothermic and downward long wave radiation is generated. So the radiation variable often reaches the peak value at last. Meanwhile, the downward long wave radiation is strongly influenced by

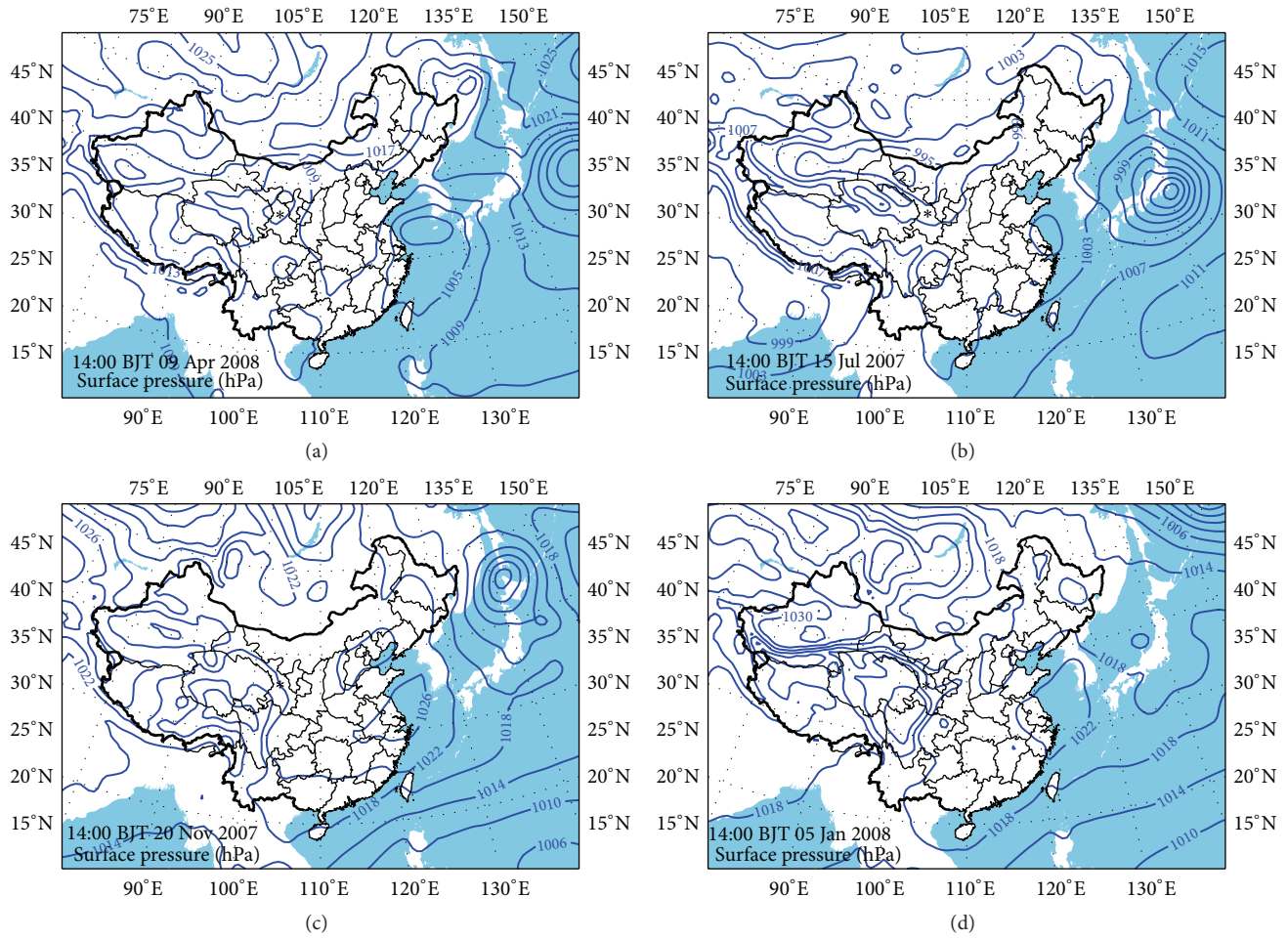

Figure 2: Surface pressure at (a) 14:00 BJT 9 April 2008, (b) 14:00 BJT 15 July 2007, (c) 14:00 BJT 20 November 2007, and (d) 14:00 BJT 5 January 2008. Black asterisk denotes measurement site.

cloudiness and air humidity. On cloudless sunny days, the downward long wave radiation is relatively low and has a weak effect on surface heating. Accordingly, Table 3 shows that downward long wave radiation is weaker, related to PBLH, than the other three radiation variables.

Figure 4 also shows variation in net radiation. Being different from the profile of temporal average of net variation in Figure 1, the net radiation has an obvious daily variation and changes consistently with short wave radiation in all cases. The variation in net radiation is the cumulative result of the components' variation in the radiation balance, but the short wave radiation is the dominant one. Therefore, the lagged law between net radiation and PBLH in different cases is similar to that between the short wave radiation and PBLH. The major factors that affect the net radiation are solar altitude angles, altitude, cloud cover, and surface albedo. The altitude and cloud cover are not considered for cloudless sunny days, and the variation in solar altitude angles is the fundamental factor to the difference on net radiation in different cases [29].

Figure 5 shows temporal variations in surface air temperature, surface infrared temperature, sensible heat flux, and surface wind speed. Relative to two temperature variables, PBLH shows a significant lag except in the case of 15 July 2007. On 17 April 2008, 20 November 2007, and 1 January 2008, the lag times are about 1, 2, and 2 hours, respectively. On 15 July 2007, two profiles increase until about 17:00 BJT and then begin to decrease, which are in line with the trend of PBLH. In summer, not only is turbulent exchange stronger, but also heat exchange between surface and atmosphere is faster, so the lagging effect of PBLH does not show very well. The temporal variation in sensible heat flux is different from others. Especially in the first two cases, the sensible heat flux even changes simultaneously with PBLH. On 20 November 2007 and 5 January 2008, PBLH changes about 1 hour later than the variable. The sensible heat flux is mainly determined by difference between surface temperature, surface air temperature, and surface wind speed. According to Figure 5, the difference between surface temperature and surface air temperature may get the peak value when the two temperature variables reach the maximum, but wind speed (red lines) keeps increasing until 18:00, which leads to the less lag time between PBLH and sensible heat flux.

The temporal variations in atmospheric pressure and surface relative humidity are shown in Figure 6, which are

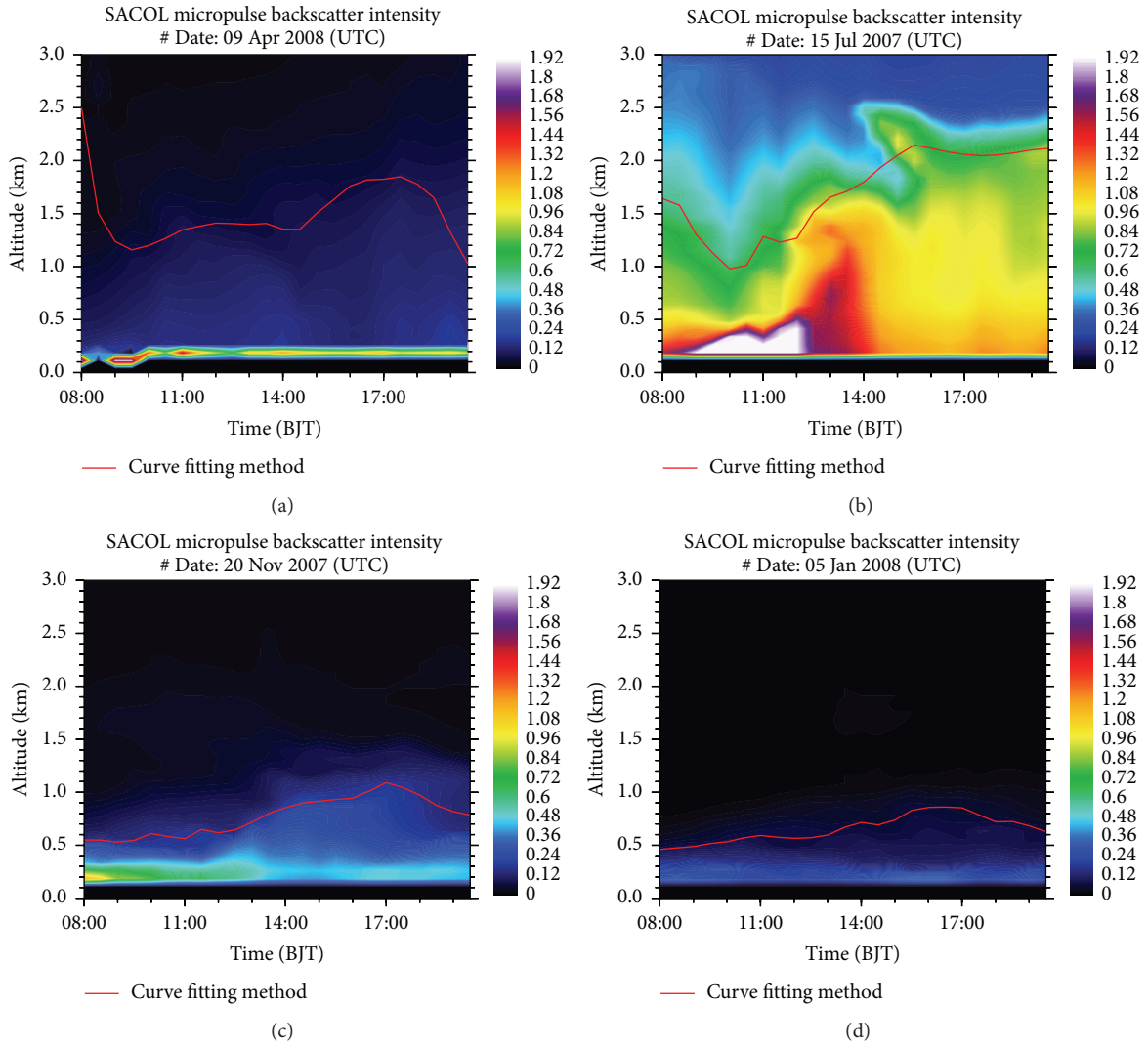

Figure 3: Time-altitude cross sections of the backscatter on (a) 9 April 2008, (b) 15 July 2007, (c) 20 November 2007, and (d) 5 January 2008.

opposite to the variations in PBLH. A comparison with the surface air temperature plotted in Figure 5 shows that the air temperature reaches its maximum at the same time as the surface relative humidity reaches its minimum, and the two quantities are highly negatively correlated. Similarly, the lag times are about 1, 2, and 2 hours on 17 April 2008, 20 November 2007, and 1 January 2008, respectively. On 15 July 2007, the relative humidity decreases until about 16:00 BJT and maintains its minimum about 17:00 BJT; then the tendency of the growth appears. For atmospheric pressure, because the variable changes weakly in all cases and the range of variation is also small, the correlation between pressure and PBLH is not as strong as between PBLH and other variables.

The above results show that in all cases of different seasons the temporal variations in all variables correspond well to that of PBLH, with upward long wave radiation, surface temperature, and surface air temperature having the closest correspondence. In the time domain, difference exists at lag time of PBLH for different cases, which is mainly caused by the seasonal variation in solar altitude angles. In addition, surface process and turbulent exchange intensity are different in different seasons. However, on the whole, to most variables, the lag times of PBLH are 2 to 3 hours. PBLH changes about 3 hours later than short wave radiation and net radiation. To upward long wave radiation, PBLH lags 2.5–3 hours. Relative to surface temperature, surface air temperature, and surface relative humidity, PBLH develops about 2 hours later. Besides, PBLH changes later than sensible heat flux less than 1 hour and consistently with atmospheric pressure. The delays in boundary layer response are related not only to the finite response times of the distribution, transformation, and transmission in the atmosphere for surface radiation energy, but also to the lag in aerosol delivery. Using lidar data, PBLH is identified by the vertical distribution of aerosol. However, upward transport of aerosol only begins after sunrise, when the boundary layer has developed in response to thermodynamic factors. In the afternoon, the true PBLH declines rapidly with the weakening of solar radiation, but the PBLH retrieved from the profile of aerosol decreases slowly. In addition, delays in

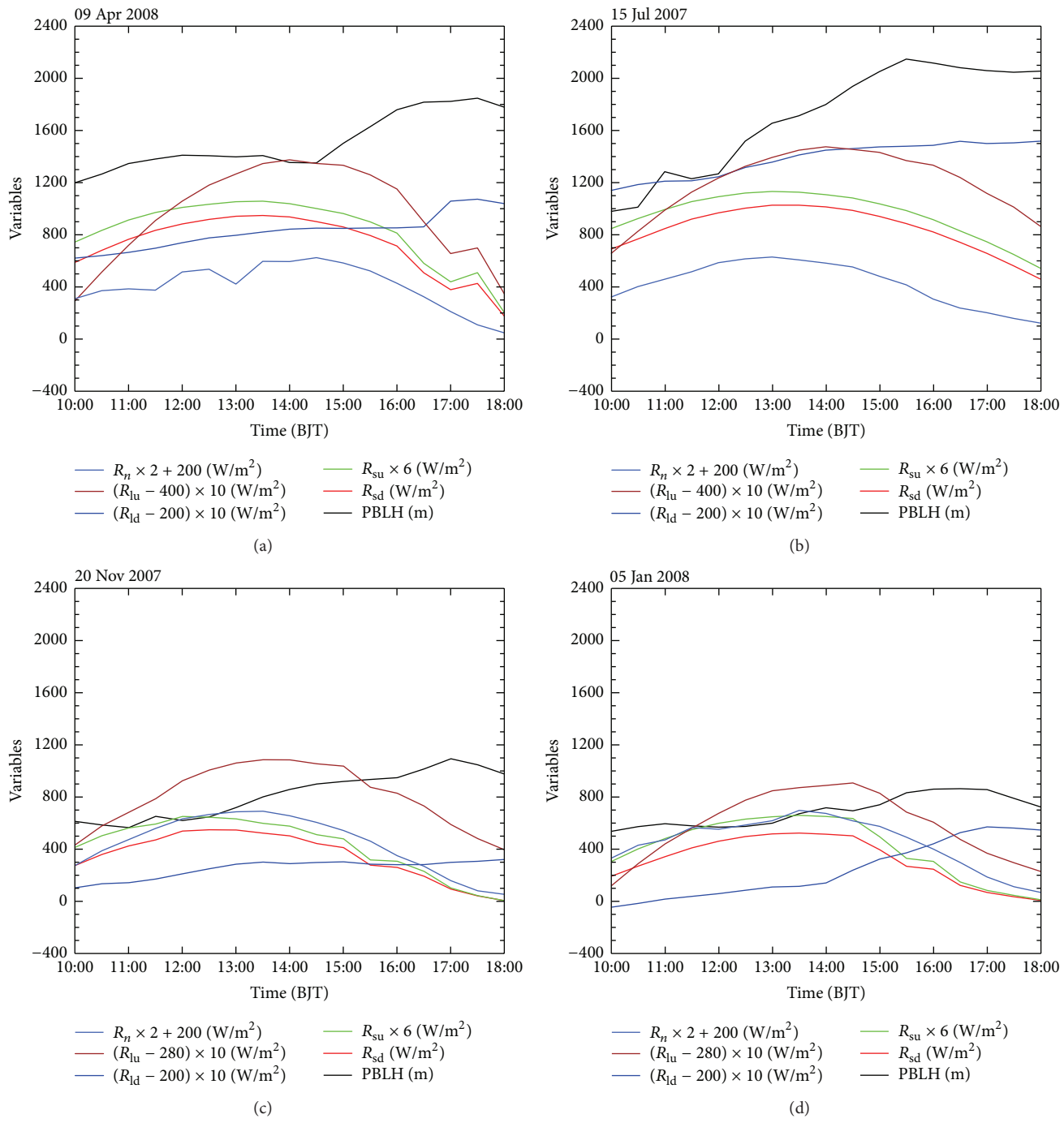

Figure 4: Temporal variations in boundary layer height (PBLH), downward short wave radiation (R_{sd}), upward short wave radiation (R_{su}), downward long wave radiation (R_{ld}), upward long wave radiation (R_{lu}), and net radiation (R_n) on (a) 9 April 2008, (b) 15 July 2007, (c) 20 November 2007, and (d) 5 January 2008.

PBLH may also reflect the influence of dynamical factors such as wind shear. Northwest China is in a region dominated by westerlies, and the atmospheric circulation background that influences the formation and development of the boundary layer has some special characteristics [30]. However, the correlation between wind shear and PBLH is not considered due to the limitations of wind data.

5. Conclusions

In this study, the statistical relationships between surface parameters and the PBLH are quantified using surface observational data and lidar-derived PBLH on 42 cloudless days from June 2007 to May 2008. The vertical dependence of PBLH on air temperature is also investigated. Then through

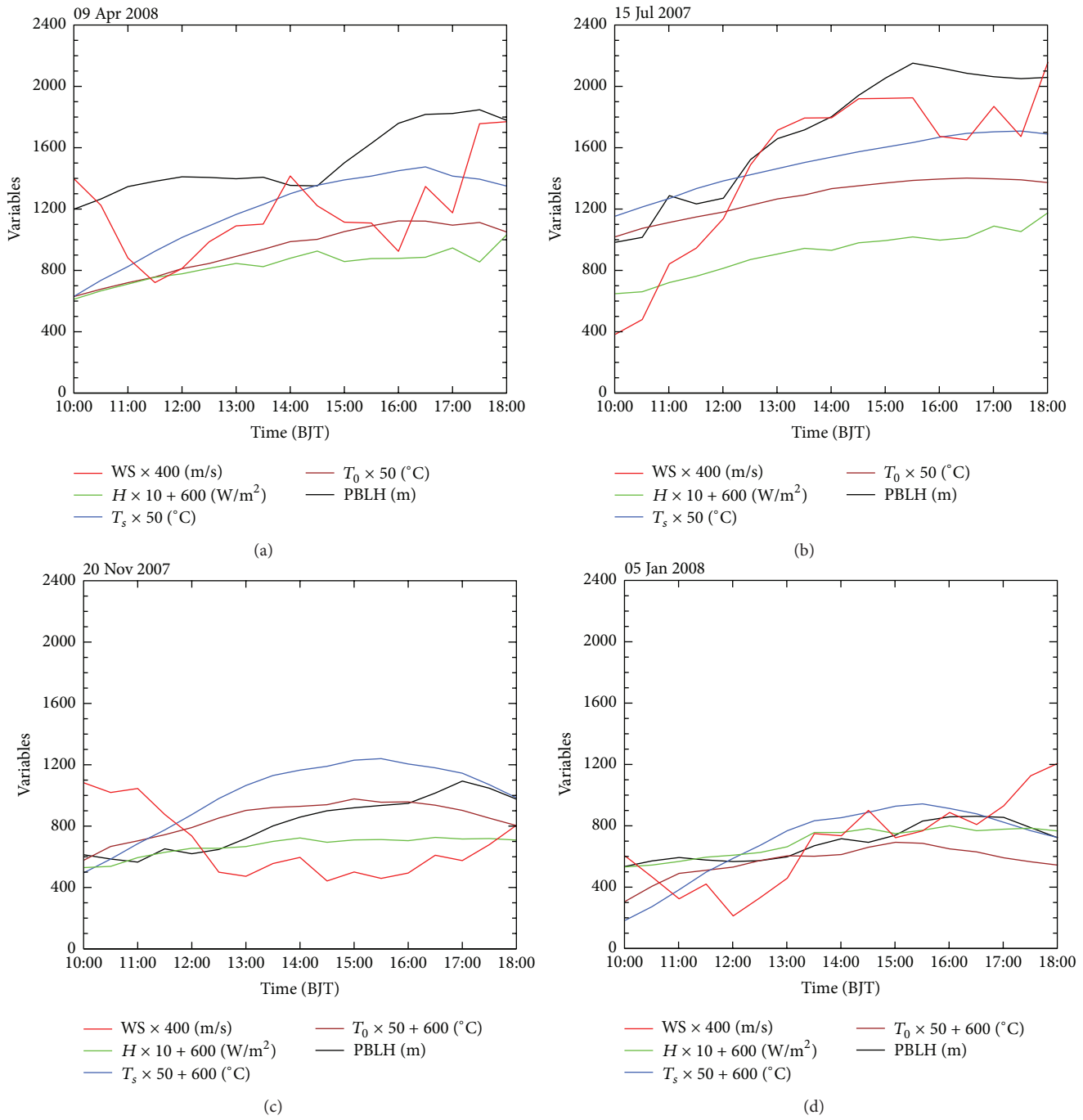

FIGURE 5: Temporal variations in boundary layer height (PBLH), sensible heat flux (H), surface temperature (T_s), surface air temperature (T_0), and surface wind speed (WS) on (a) 9 April 2008, (b) 15 July 2007, (c) 20 November 2007, and (d) 5 January 2008.

temporal variations on the four typical cases 15 July 2007, 20 November 2007, 5 January 2008, and 9 April 2008 in different seasons, the lagged laws between different variables and PBLH, as well as the physical mechanisms behind statistical correlations, are specifically discussed. The conclusions of the study are as follows.

(1) Among the atmospheric variables (not including dynamic factors), thermal variables such as radiation variables, surface temperature, and sensible heat flux have significant positive correlations with PBLH. The response time to thermal forcing of the surface and atmosphere, together with aerosol transmission delay, means that the development of the boundary layer lags behind changes in the driving variables with different lag times for different variables.

(2) On different cases, the lag correlation laws between PBLH and variables are different (especially on 15 July 2007). But on the whole, only downward long wave

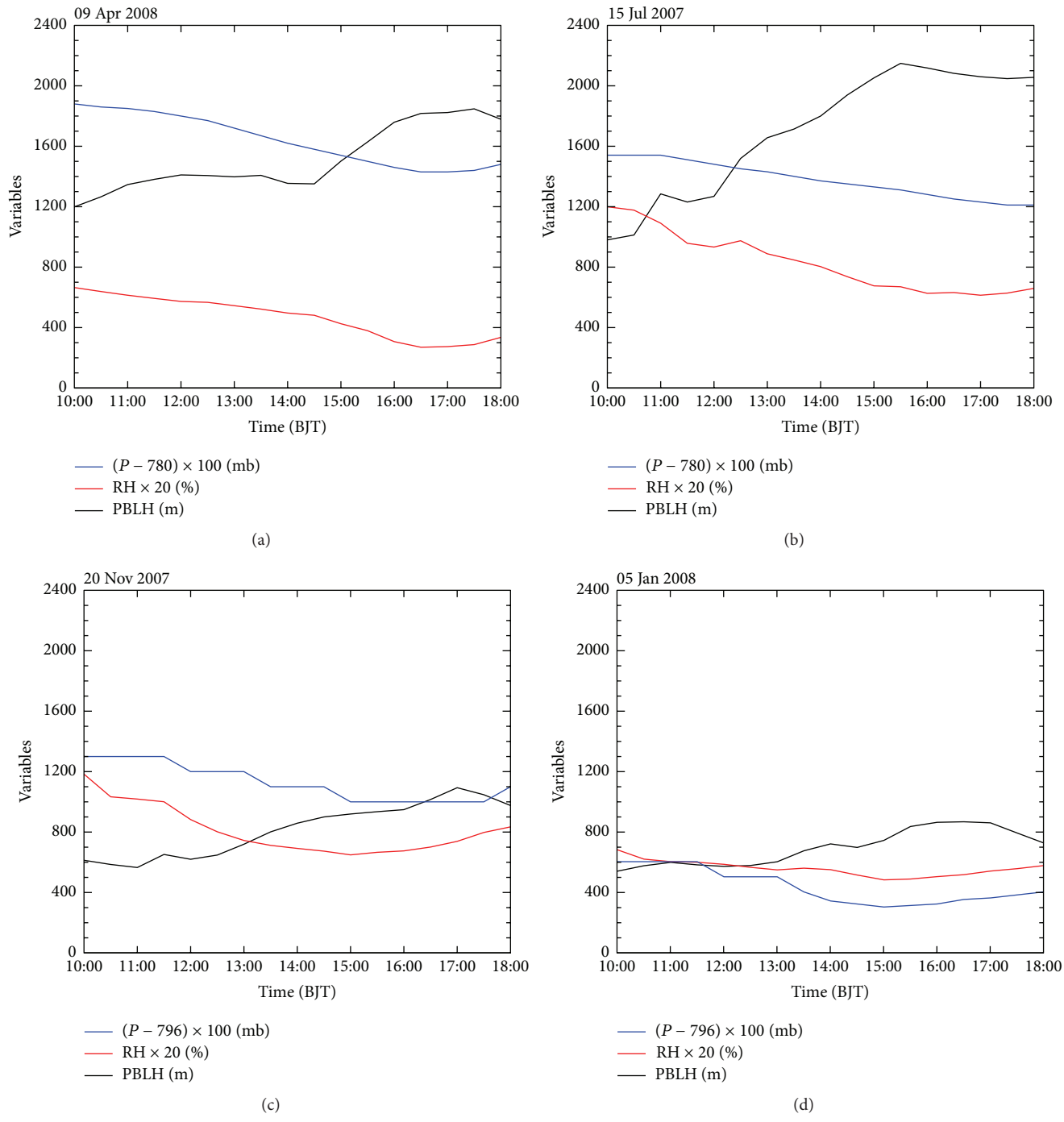

FIGURE 6: Temporal variations in boundary layer height (PBLH), surface relative humidity (RH), and atmospheric pressure (P) on (a) 9 April 2008, (b) 15 July 2007, (c) 20 November 2007, and (d) 5 January 2008.

radiation changes synchronous with PBLH. Changes in the boundary layer occur 3 hours later than changes in downward and upward short wave radiation, upward long wave radiation, and net radiation. The lag time of PBLH is about 2 hours relative to surface temperature and surface air temperature, and PBLH lags behind surface sensible heat flux about 1 hour.

(3) Surface relative humidity and atmospheric pressure are weakly negative correlative to PBLH. PBLH changes about 2 hours later than surface relative humidity.

(4) The vertical dependence of PBLH on air temperature is greatest near the surface and decreases with height.

The most significant correlation between air temperature below (above) 1000 m and PBLH occurs at 12:00 (14:00) BJT.

Although above important conclusions have been gotten, there are still several unresolved problems. Firstly, curve fitting is an effective method for calculating PBLH with lidar data but is limited to cloudless sunny days. The number of cases and their seasonal distribution are constrained by data availability. While the statistical results are representative they also have some limitations. Secondly, as a major dynamical factor, wind shear affects the thermal transmission and diffusion capacity of the atmosphere and is significantly correlated with the development of the boundary layer in theory. However, the variable is not considered here because of the limited amount of available data. This analysis is focused on determining the statistical correlation between PBLH and conventional atmospheric variables based on routine observations at SACOL and providing basis and support for the assimilation of PBLH in numerical weather predictions over the Northwest China. But for the study understanding and awareness about how the meteorological conditions affect the development of the boundary layer in the Yuzhong area are not deep enough.

Competing Interests

The authors declare that there are no competing interests regarding the publication of this paper.

Acknowledgments

The authors would like to thank the Semi-Arid Climate and Environment Observatory of Lanzhou University (SACOL) for providing the observation data. This research was supported by the National Natural Science Foundation of China (Grant no. 41375109) and Arid Meteorology Science Foundation of Institute of Arid Meteorology, China Meteorological Administration (Grant no. IAM201513).

References

[1] R. B. Stull, *An Introduction to Boundary Layer Meteorology*, Springer Science & Business Media, 1988.

[2] Q. Zhang, "Review of atmospheric boundary layer meteorology," *Arid Meteorology*, vol. 21, no. 3, pp. 74–78, 2003.

[3] X.-M. Hu, J. W. Nielsen-Gammon, and F. Zhang, "Evaluation of three planetary boundary layer schemes in the WRF model," *Journal of Applied Meteorology and Climatology*, vol. 49, no. 9, pp. 1831–1844, 2010.

[4] S.-E. Gryning and E. Batchvarova, "Parametrization of the depth of the entrainment zone above the daytime mixed layer," *Quarterly Journal of the Royal Meteorological Society*, vol. 120, no. 515, pp. 47–58, 1994.

[5] A. B. White, C. W. Fairall, and D. W. Thomson, "Radar observations of humidity variability in and above the marine atmospheric boundary layer," *Journal of Atmospheric and Oceanic Technology*, vol. 8, no. 5, pp. 639–658, 1991.

[6] K. J. Davis, N. Gamage, C. R. Hagelberg, C. Kiemle, D. H. Lenschow, and P. P. Sulivan, "An objective method for deriving atmospheric structure from airborne lidar observations," *Journal of Atmospheric and Oceanic Technology*, vol. 17, no. 11, pp. 1455–1468, 2000.

[7] B. Hennemuth and A. Lammert, "Determination of the atmospheric boundary layer height from radiosonde and lidar backscatter," *Boundary-Layer Meteorology*, vol. 120, no. 1, pp. 181–200, 2006.

[8] K. L. Hayden, K. G. Anlauf, R. M. Hoff et al., "The vertical chemical and meteorological structure of the boundary layer in the Lower Fraser Valley during Pacific '93," *Atmospheric Environment*, vol. 31, no. 14, pp. 2089–2105, 1997.

[9] V. Wulfmeyer, "Investigation of turbulent processes in the lower troposphere with water vapor DIAL and radar-RASS," *Journal of the Atmospheric Sciences*, vol. 56, no. 8, pp. 1055–1076, 1999.

[10] S. A. Cohn and W. M. Angevine, "Boundary layer height and entrainment zone thickness measured by lidars and wind-profiling radars," *Journal of Applied Meteorology*, vol. 39, no. 8, pp. 1233–1247, 2000.

[11] I. M. Brooks, "Finding boundary layer top: application of a wavelet covariance transform to lidar backscatter profiles," *Journal of Atmospheric and Oceanic Technology*, vol. 20, no. 8, pp. 1092–1105, 2003.

[12] H. Li, Y. Ma, and Y. Yang, "Study on retrieval of boundary layer using wavelet transformation method based on Lidar data," *Arid Meteorology*, vol. 33, no. 1, pp. 78–88, 2015.

[13] W. P. Hooper and E. W. Eloranta, "Lidar measurements of wind in the planetary boundary layer: the method, accuracy and results from joint measurements with radiosonde and kytoon," *Journal of Climate & Applied Meteorology*, vol. 25, no. 7, pp. 990–1001, 1986.

[14] D. G. Steyn, M. Baldi, and R. M. Hoff, "The detection of mixed layer depth and entrainment zone thickness from lidar backscatter profiles," *Journal of Atmospheric and Oceanic Technology*, vol. 16, no. 7, pp. 953–959, 1999.

[15] L. Wang, C. Xie, Y. Han, D. Liu, and H. Wei, "Comparison of retrieval methods of planetary boundary layer height from lidar data," *Journal of Atmospheric and Environmental Optics*, vol. 7, no. 4, pp. 241–247, 2012.

[16] L. Wang, C. Xie, Z. Wang et al., "Application of gradient method to detect height distribution of atmospheric boundary layer with lidar," *Journal of Atmospheric and Environmental Optics*, vol. 7, no. 3, pp. 161–167, 2012.

[17] C. Huang, X. Song, and Z. Liu, "Development of atmospheric boundary layer detection based on lidar data," in *Proceedings of the Chinese Optical Society Conference*, Beijing, China, 2010.

[18] Y. Hu and Y. Gao, "Some new knowledge to land surface processes in arid region," *Acta Mechanica Sinica*, vol. 52, no. 3, pp. 285–296, 1994.

[19] T. Tang, L. Wang, and X. Wen, "A study of the radiation and surface energy balance around the Ngoring Lake in source regions of the Yellow River," *Journal of Glaciology and Geocryology*, vol. 35, no. 6, pp. 1462–1473, 2013.

[20] Q. Zhang and X. Cao, "The influence of synoptic conditions on the averaged surface heat and radiation budget energy over desert or gobi," *Chinese Journal of Atmospheric Sciences*, vol. 27, no. 2, pp. 245–254, 2003.

[21] J. Qiao, *The Temporal and Spatial Characteristics of Atmospheric Boundary Layer and Its Formation Mechanism over Arid Region of Northwest China*, Chinese Academy of Meteorological Sciences, Beijing, China, 2009.

[22] Q. Zhang, J. Zhang, J. Qiao et al., "Relationship of atmospheric boundary layer depth with the thermodynamic processes at the land surface in arid regions of China," *Science China Earth Sciences*, vol. 41, no. 9, pp. 1365–1374, 2011.

[23] J. Zhang, Q. Zhang, and C. Tang, "Temporal variety of boundary layer height over deep arid region and the relations with energy balance," *Acta Ecologica Sinica*, vol. 33, no. 8, pp. 2545–2555, 2013.

[24] C. Zhao, S. Lv, Z. Li et al., "Numerical simulation of influence of land surface thermal condition on Badain Jaran desert atmospheric boundary layer height in summer," *Plateau Meteorology*, vol. 33, no. 6, pp. 1526–1533, 2014.

[25] E. J. Welton, J. R. Campbell, J. D. Spinhirne, and V. S. Scott, "Global monitoring of clouds and aerosols using a network of micropulse lidar systems," in *Proceedings of the Lidar Remote Sensing for Industry and Environment Monitoring*, vol. 4153 of *Proceedings of SPIE*, pp. 151–158, Sendai, Japan, October 2001.

[26] Z. Huang, J. Huang, J. Bi et al., "Dust aerosol vertical structure measurements using three MPL lidars during 2008 China–US joint dust field experiment," *Journal of Geophysical Research: Atmospheres*, vol. 115, no. 7, Article ID D00K15, 2010.

[27] H. Ding, *Measurements of Aerosol Vertical Profiles and the Mixed Layer Height Using a Micro Pulse Lidar*, Nanjing University of Information Science & Technology, Nanjing, China, 2012.

[28] S. Zhao, L. Zhang, Z. Wang, T. Wang, L. Zhang, and J. Liang, "Boundary layer height estimate in summer over the Lanzhou suburb in the Yuzhong area using lidar measurement and numerical model," *Climatic and Environmental Research*, vol. 17, no. 5, pp. 523–531, 2012.

[29] R. Wu and Y. Ma, "Comparative analyses on radiation characteristic in different areas over the tibetan plateau," *Plateau Meteorology*, vol. 29, no. 2, pp. 251–259, 2010.

[30] Q. Zhang and S. Wang, "A study on atmospheric boundary layer structure on a clear day in the arid region in Northwest China," *Acta Meteorologica Sinica*, vol. 66, no. 4, pp. 599–608, 2008.